CHAPTER IV

PHOTOLUMINESCENCE SPECTROSCOPY

4.1 Photoluminescence

As mentioned in the Chapter II, photoluminescence (PL) is a well-known process and an important physical phenomenon used to characterize semiconductor structures. The main idea of PL spectroscopy is investigating the transition of photogenerated carriers between the valence-band and conduction-band states and the results reflect the conduction-band and valance-band structures, the dynamics of the carrier relaxation and recombination, the excitonic and the many-body effects, etc. [54-59]. However, the PL spectrum, which gives a number of such important information, is sometimes difficult to extract. In brief, PL occurs when a sample absorbs light of some wavelength and emits light at a specific wavelength depending on the material's specific structure, composition, and quality. This chapter will further describe the nature of photoluminescence, in relation to semiconductor materials, and its use in understanding structures under investigation.

This section first describes physics of PL by using the simplest electron picture. Then, a description using electron and hole energy bands and excitons will be examined. This more complicated description helps explain PL features of samples with complicated structures, such as those examined in this thesis work.

Photoluminescence is one of optical luminescence techniques which involve a system excited by electromagnetic (EM) radiation. Lasers can provide sufficient power to excite the carriers in the sample. Typically, the incident light used to excite the sample comes from a laser source with energy of $\hbar\omega_{laser}$. As the incident light (EM radiation) strikes on the sample, it causes electrons to jump up into excited states, as shown in Fig. 4.1, which is a typical energy diagram used to explain this process. When an excited electron returns to its initial state, it may generate a photon with energy $\hbar\omega_{PL}$ (and possibly multiple phonons with combined energies of $\hbar\Omega_{phonon}$) [60-64]. Due to the law of energy conservation, this can be expressed as

$$\hbar\omega_{laser} = \hbar\omega_{PL} + \hbar\Omega_{phonon} \tag{4.1}$$

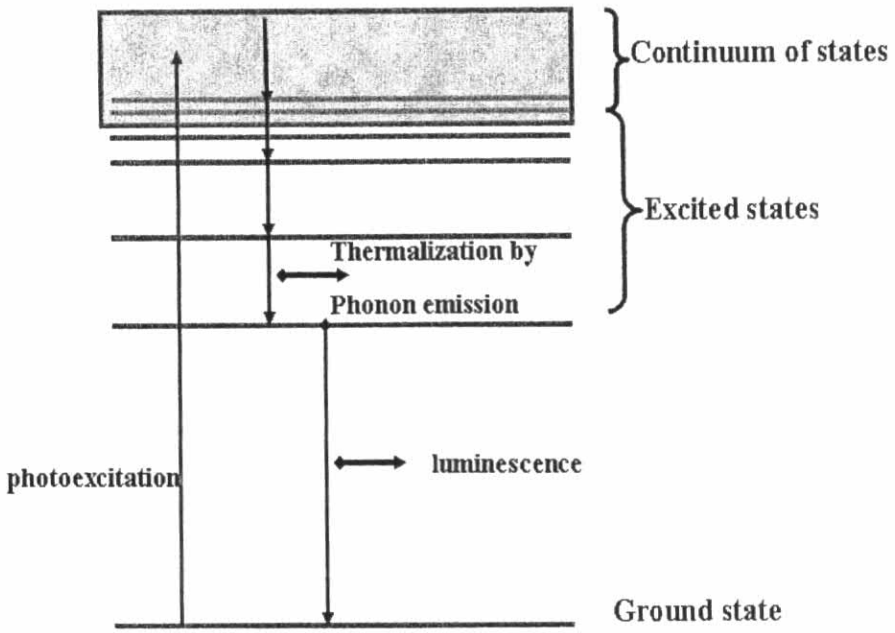

Figure 4.1 A typical energy diagram for electron system. As the incident light (EM radiation) strikes on the sample, it causes electrons to jump up into excited states.

Continuous-wave (cw) laser excitation was used to excite all samples in this thesis work. In this case, luminescence can be considered as a steady-state phenomenon, that is, the sample interacts with the excitation source and emits light continuously. The first part in the above process is optical absorption of the incident light. The amount of photon absorption by the material depends on the incident photons' wavelength (energy) of the source of excitation. Eq. 4.2 addresses the theoretical prediction of the absorption coefficient α for a direct-bandgap semiconductor.

$$\alpha = A(\hbar\omega + E_{gap})^p = A(\frac{\hbar c}{\lambda} + E_{gap})^p \qquad (4.2)$$

where A and p are constants for the particular material, $\hbar\omega$ is the photon energy of the laser light, and E_{gap} is the bandgap energy of the structure under excitation. Once the optical absorption has excited an electron to a higher energy state, the electron can relax to a lower energy state. Different processes may take part in this relaxation, which can be categorized as either *radiative processes* (such as PL) or *non-radiative processes* (such as phonon emission, capture by deep centers, or the Auger effect).

The rate of emission for radiative recombination depends on the amount of electron excitation via the absorption of this light. Eq. 4.3 explains the recombination process of the PL.

$$R = n_i n_f P_{if} \tag{4.3}$$

where n_i and n_f are the density of initial and final (empty) states, respectively; and P_{if} is the probability of a transition from the initial state to the final state.

Generally, the higher-energy excitation causes more phonons to be emitted before the luminescence occurs. Similarly, lower excitation energy tends to induce fewer phonon emissions. If the excitation energy is less than the energy difference between the ground state and the first excited state, then no optical absorption will occur, resulting in no PL. The above electron picture is not sufficient to explain many PL characteristics seen in structured semiconductors. A better explanation considers the optical absorption as a transition from the valence band to the conduction band. Emission then entails the movement of an electron from the minima of the conduction band to the maxima of the valence band. The optical absorption across bandgaps for a direct-bandgap material and an indirect-bandgap material are both shown in Fig. 4.2. As described in the Chapter II, the conduction band and the valence band correlate to free carriers, that is, electrons and holes, respectively. In fact, photoluminescence (Fig. 4.3) can be considered as the radiative recombination of conduction-band electrons with valence-band holes in semiconductors. When the excitation energy is less than the bandgap energy, no optical absorption will occur, and hence no PL.

PL can be observed from samples with structures that are more complicated in composition than just a bulk semiconductor material. It can be used to investigate how well the samples are grown, and to verify the material composition. This is because the energy differences measured by PL change with impurities and structures, as illustrated in Figs. 4.2, 4.3 and 4.4.

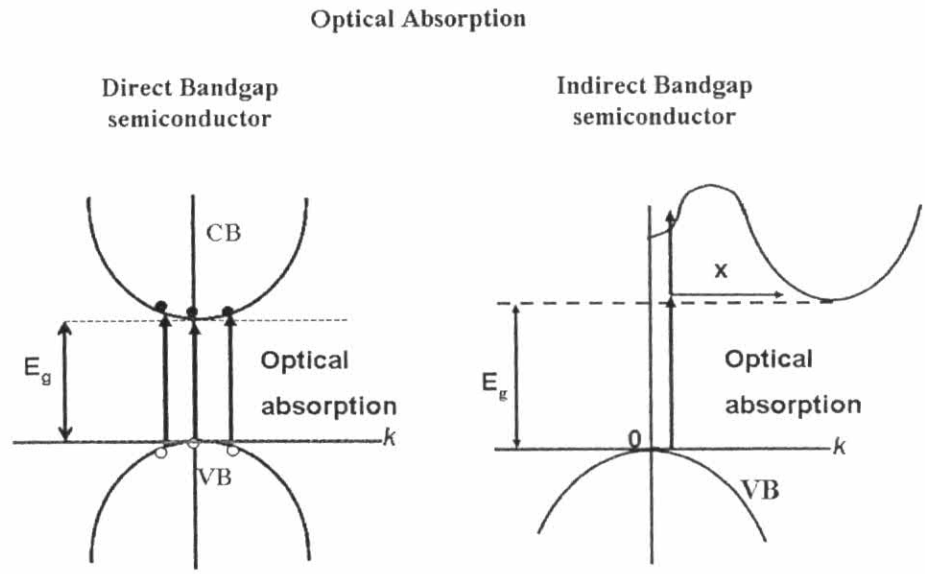

Figure 4.2 A typical energy absorption diagram in direct- and indirect-bandgap semiconductors: As the incident light (EM radiation) strikes on the sample, it causes electrons to jump up from the valance band into the conduction band. (After P. Bhattacharya, *Semiconductor Optoelectronic Devices*)

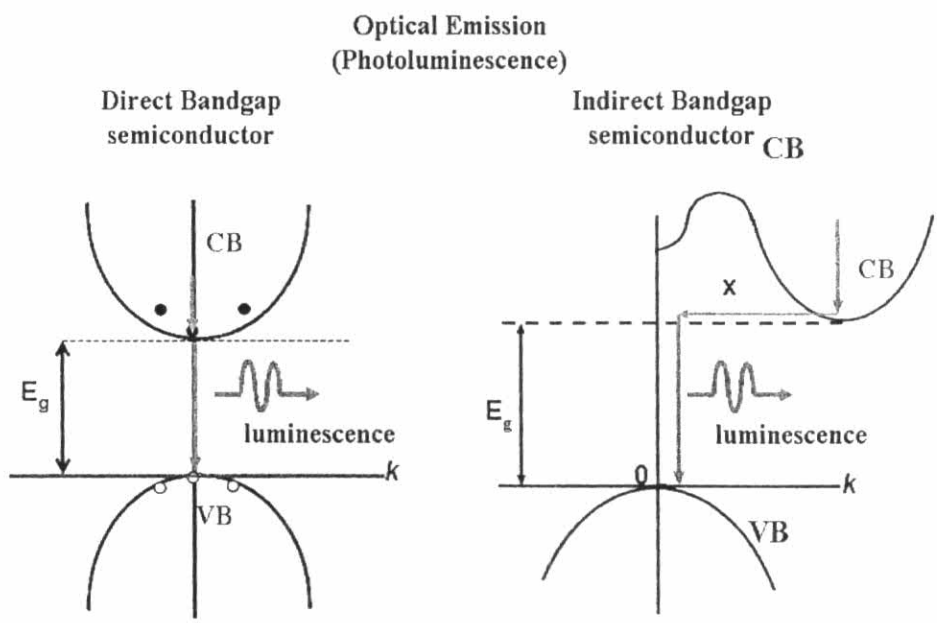

Figure 4.3 A typical energy emission diagram in direct- and indirect-bandgap semiconductors: As electrons come back to the initial state in the valence band, the electron and the holes recombine and emit photoluminescence (After P. Bhattacharya, *Semiconductor Optoelectronic Devices*)

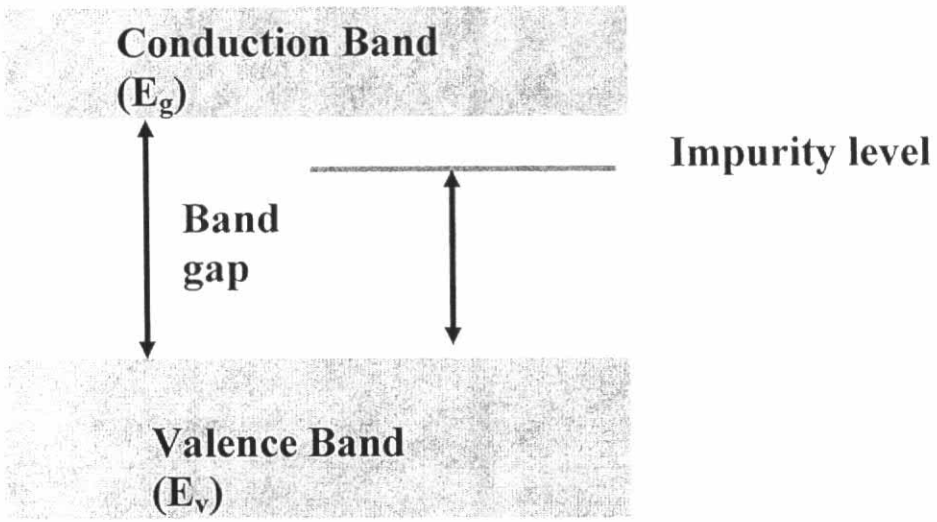

Figure 4.4 Bandgap energy changes due to impurity and other effects (After M. A. Omar, *Elementary Solid State Physics*)

4.2 Optical Excitation

With laser light to be used in the PL spectroscopy, three parameters must be considered: wavelength (excitation energy), intensity (excitation power), and polarization. There are two ways to optically excite quantum dots. These are *non-resonant excitation*, and *resonant excitation*.

In non-resonant excitation, which corresponds to excitation above GaAs bandgap in our case (Fig. 4.5), the energy of the laser was tuned above the GaAs bandgap, in particular, 1.87 eV (660 nm) was used. Electrons and holes were thus generated in the GaAs matrix surrounding the InAs quantum dots. In a random manner, a fraction of these carriers were captured first by the *wetting layer*, which behaves as a thin quantum well. They then fell into the higher excited states of quantum dots, finally most of them reached the electron and hole ground states before recombining. For weak excitation, the dominant intraband relaxation mechanism inside the quantum dot is thought to be phonon emission [52], although the relaxation rates typically seen are faster than theoretically expected. When the carrier density is higher, Auger processes (multi-carrier scattering) can also manifest. Above-bandgap excitation is convenient for several reasons. First, it is relatively efficient, since a large area of GaAs acts as the absorber and funnels the carriers into the quantum dots. For continuous-wave (cw)

excitation, appropriate pump powers were often just tens of microwatts in the setup used in this work. Also, since the laser wavelength (often 650 nm or 700 nm) was far detuned from the quantum-dot emission wavelength (900 nm), the reflected laser light passing through the beam splitter, which was in the same direction as the luminescence, was easily rejected using a color filter with 90% efficiency at the emission wavelength. Finally, by increasing the laser power, it was straightforward to investigate the multi-particle states of a quantum dot.

In resonant excitation, the laser is tuned to a higher transition energy within the quantum dot, as shown also in Fig. 4.5. A much larger laser power is required than for the above-band excitation, since the absorption cross-section of a single quantum dot is very small. In this thesis, all measurements were done under the non-resonant excitation (above-bandgap excitation).

The intensity of the PL signal depends on the excitation laser power also. The intensity of the excitation beam (the power of the laser) affects the PL peak intensity in a linear fashion until a saturation intensity is reached. Although this general description applies to all samples, the point at which these different features occur is sample-dependent.

In the non-resonant excitation above the GaAs bandgap used in this thesis work, the laser had the photon energy higher than the GaAs bandgap energy. The laser excited the carriers within the barrier region and diffused towards the InAs QDs in order to be captured and consequently relax and recombine at the QD ground energy state. Because the spin-flip process occurred in the GaAs region, the carriers did not have enough memory to recognize the polarization state of the excitation laser. Therefore, the measured polarization state of aligned quantum dot arrays was independent of that of the excitation source.

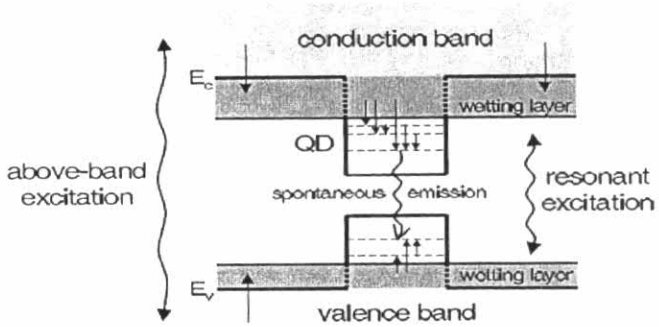

Figure 4.5 Non-resonant optical excitation. (After C. M. Santori, *Generation of Nonclassical Light Using Semiconductor Quantum Dots*)

4.3 Macro-Photoluminescence

The main tool for optical characterization in this research work was the photo-luminescence (PL) spectroscopy. A schematic of the macro-PL experimental setup is shown in Fig. 4.6. The samples were excited by the 514-nm line of an Ar^+ laser. The PL signal was resolved by a 1-meter monochromator. Typically, the entrance and the exit slit widths are 0.5 mm. The resolved light signal was detected by a liquid-N_2-cooled InGaAs detector (Hamamatsu's G7754-01 with 0.1-mm^2 active area). An optical beam chopper and the associated lock-in amplifier were used to enhance the signal by the standard lock-in technique. For low-temperature and temperature-dependent measurements, the sample was mounted on the cold finger of a closed-cycle cryostat.

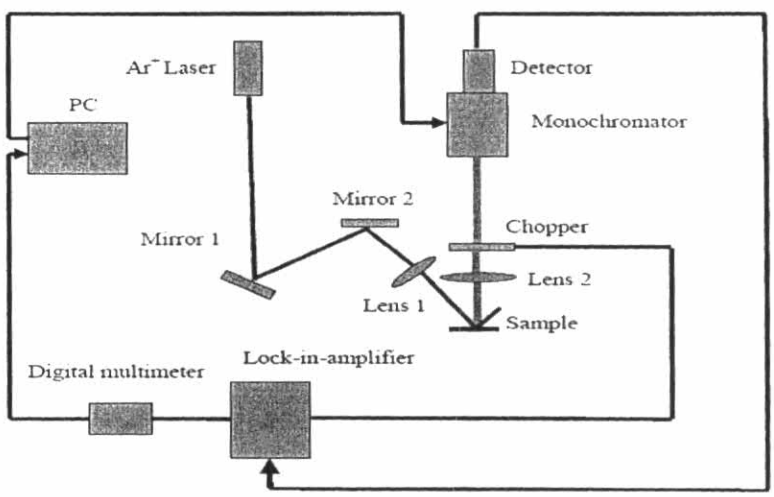

Figure 4.6 Macro-photoluminescence setup.

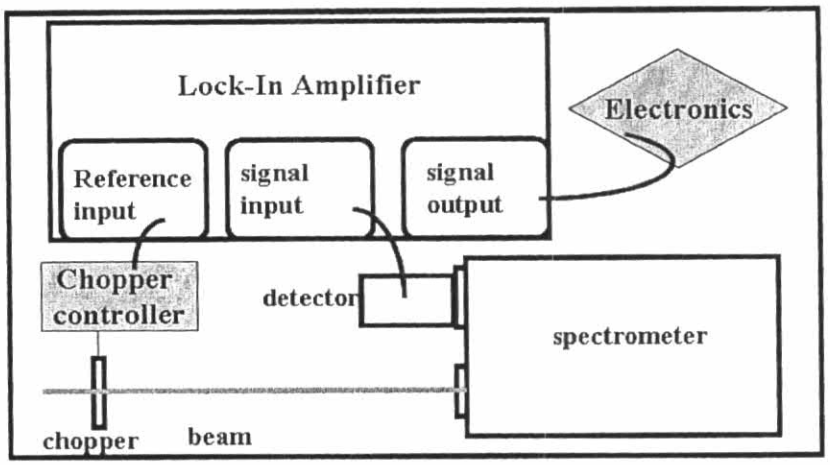

Figure 4.7 Standard lock-in technique.

Figure 4.7 shows the function and the essential parts of the lock-in technique. An optical chopper renders the optical beam into a series of square-wave pulses. This can be positioned either close to the laser source or immediately after the sample. With earlier placement of the chopper in the optical path, less noise is included in the chopped beam. This detection technique averages away any random non-chopped signal. The chopper controller sends a reference signal (square wave with the frequency that the beam is being chopped) to the lock-in amplifier. This sets the frequency to be detected by the lock-in and fixes the timing of the signal to allow phase-sensitive detection to occur.

4.4 Micro-Photoluminescence

4.4.1 Cryogenics

All the samples were held in a continuous-flow liquid-helium cryostat. A diagram of a typical continuous-flow cryostat is as shown in Fig. 4.8. The cryostat itself was mounted on a fairly steady two-axis translation stage, which allowed horizontal and vertical adjustments of the cryostat position. The sample was attached to a cold finger in a vacuum chamber.

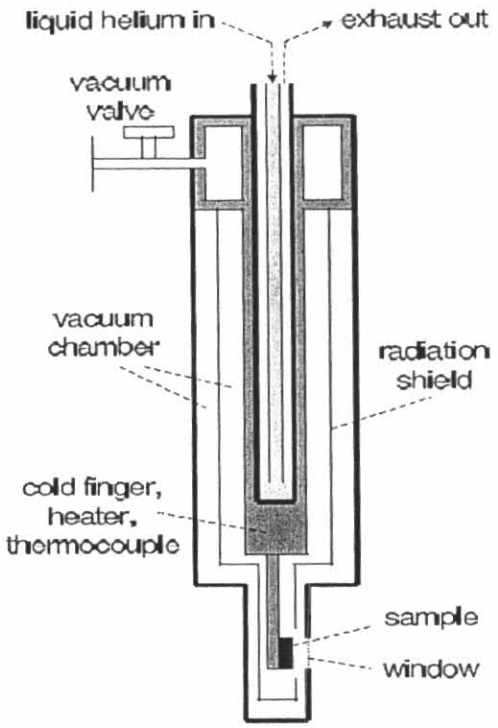

Figure 4.8 Cross-section of the cryostat.

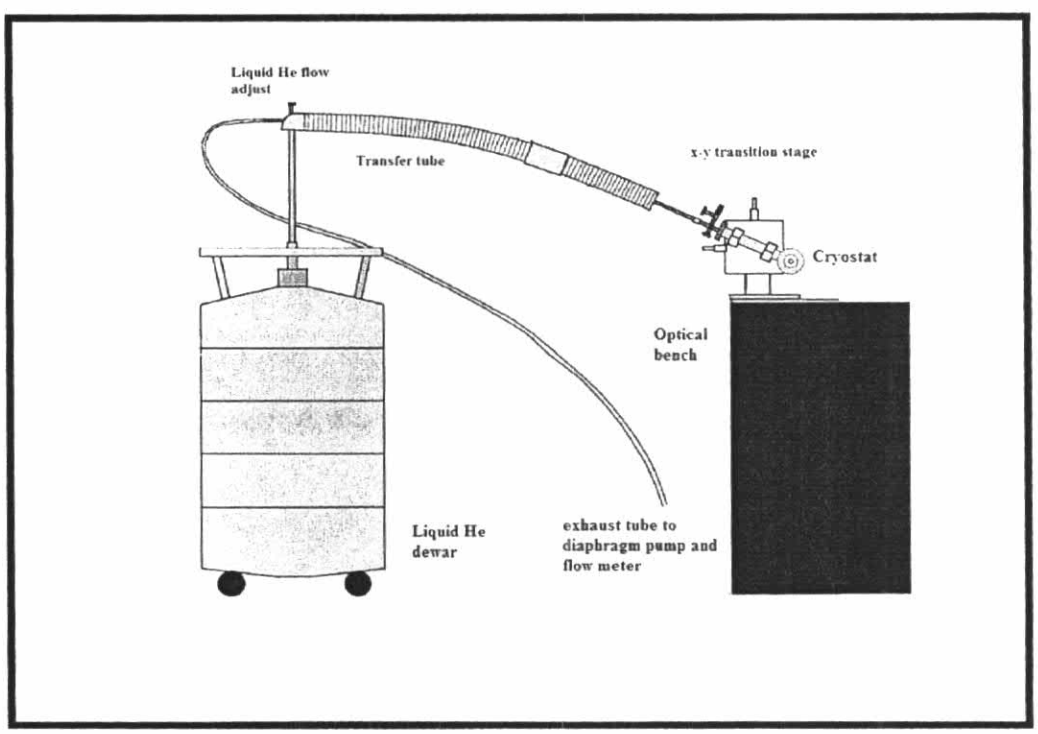

Figure 4.9 (a) A schematic diagram of the cooling system for the sample.

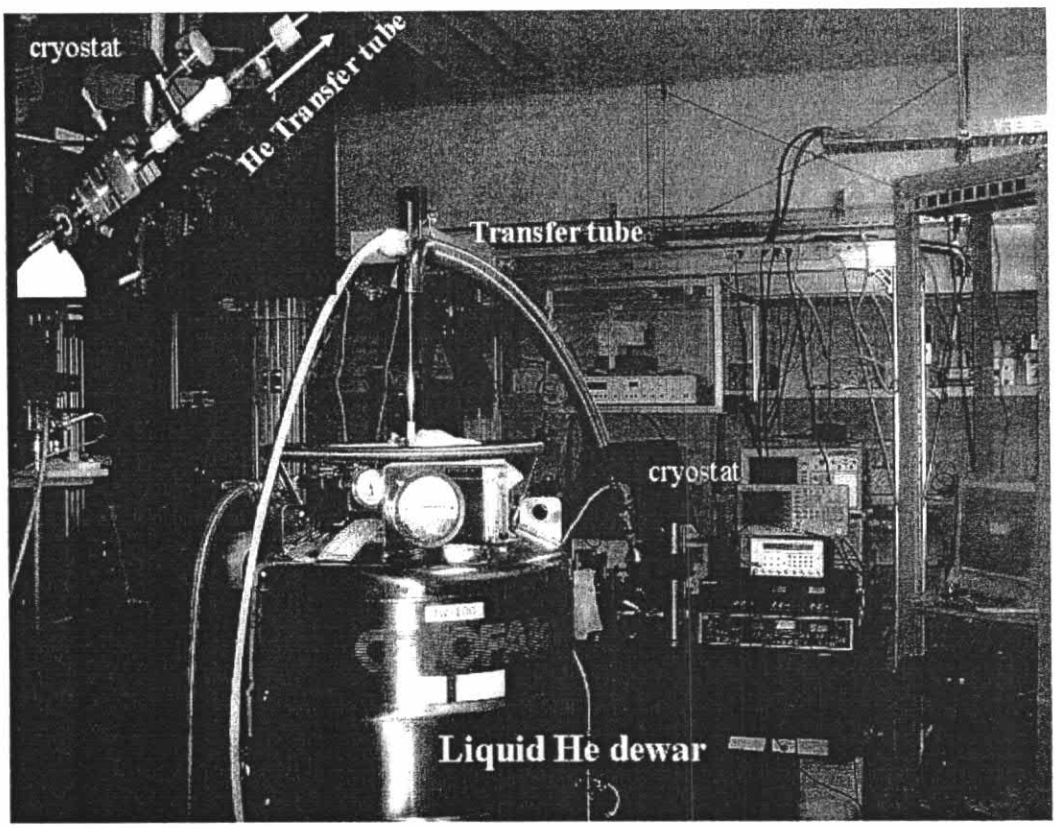

Figure 4.9 (b) Photo of the cooling system for the sample used in this work.

Liquid helium was delivered from a dewar, through a transfer tube, to the inside of the cold finger. The helium waste gas then exited from the cryostat. A window in the outside of the vacuum chamber allowed optical access to the sample. For this cryostat, the waste helium was pumped out through an outer shield of the transfer tube, so that the incoming helium was insulated, enhancing the measurement efficiency. The helium consumption rate for this cryostat could be around 1 L/hr.

4.4.2 Optical Setup

Measuring the light emission from an aligned quantum dot system can be done with a standard procedure. The essential components of the setup including the excitation part for sample and the part used to collect emission from quantum dots are shown in Fig. 4.11 (a) and (b). Only one 45%:45% beam splitter was used for all of the optical excitation path, the emission path and the illumination path. For the excitation part, 45% of the laser transmitted from the beam splitter was incident on the sample. The laser excitation was usually applied for normal excitation on the sample. By doing so, the first advantage was that the optical path of the laser and of the luminescence was the same. Also, the alignment for the emission part could be easily done. The laser spot size on the sample was typically about 1 to 2 μm in diameter. At the same time, 45% of the pump laser was passed through the beam splitter and was incident upon the photodetector. The amount of the laser light impinging on the photodetector, measured by an optical power meter, was the same amount as that of the laser which stroke upon the sample. By measuring the laser spot on the photodetector, the amount of laser that was incident upon the sample could be known. The semiconductor laser used in this setup provided a wavelength in the red-wavelength region of 660 nm. The highest optical power of the laser used was 60 mW.

An illumination technique was used to visualize the sample during the experiment (see Fig. 4.10). Light coming from the light source was captured by the first lens to produce a collimated beam, and then passed into a diaphragm. By adjusting the aperture of the diaphragm, the amount of light could be controlled. For the illumination part, the second lens helped to focus the light at the back of the objective lens after passing through a beam splitter. After passing through the objective lens, the light impinged on the sample. After that, the light reflected back from the sample came back in the same direction as the incident light. Another beam splitter (which is normally used with the visible light region) in the illumination optic path sent about half of the light to another path to the CCD camera. The third lens in front of the camera focused the reflected light from the sample to the slit of the CCD camera. Alignment of the optical components utilizing a microscope to optimize illumination was carried out following the Kohler illumination rules. The laser beam shape, size, and location on the sample were checked by monitoring the reflection

image on the CCD camera, on which the laser beam was illuminated together with a white light illumination by a tungsten lamp.

The emission from the sample was reflected in the same direction as the excitation laser through an objective lens, whose numerical aperture was 0.45 and focal length was 200 mm. There was a flip-mirror that sent the luminescence to the spectrometer, and the illumination light from the light source was already blocked by flipping up the mirror.

Another lens (focal length of 5cm) was placed in front of the spectrometer to collect all the PL emission. The purpose of placing this lens in front of the spectrometer was to collect all PL signal and focusing it to the spectrometer, and the *f*-number of this lens must match with that of the spectrometer. It was advantageous to insert two lenses after the sample so that the light emission after passing through the microscopic lens could create parallel rays, allowing Lens 2 (L2) to easily focus the light signal onto the spectrometer's slits. Lens 2 (L2) was placed on a hinge mount in order to be easily adjusted. Although it was assumed that the PL emission was from a point source, adjustment of the objective lens was not possible in this setup, however, since the lens L2 could always focus two parallel rays. For instance, the signal emitted from the sample could be affected by both the thickness and whether the signal originated from deep within the sample or near the surface, depending on the sample under investigation. Also, the index of refraction, which affected the divergence of the PL signal leaving the sample, was also sample-dependant. Hence, only L2 was needed to be moved to compensate for different samples' effects, without changing the position of objective lens. Therefore, this two-lens configuration facilitated matching the spectrometer's *f*-number and focusing the PL signal into the spectrometer.

In addition to the lenses shown in the above figures, it was practical to have multiple apertures in the system for alignment purposes, as shown in Fig. 4.11. Although these were meant to be static parts of the experiment, they could be moved and changed as needed. These apertures could block some of the laser light from reaching the sample; thus, their position and size would change the eventual intensity impinging on the sample. It is important for the user to be aware of the multiple

components in the system and the effect they have on the actual optical intensity reaching the sample.

Optical filters are another component that will affect the overall outcome of the experiment. The two most common types of filters used are neutral density (ND) filters and color filters. Figure 4.11 shows a color filter placed in front of the spectrometer's slit and an ND filter in front of the laser light before striking the sample. ND filters uniformly reduce the intensity of light over a relatively broad wavelength range. Moreover, the power incident on the sample was varied by introducing ND filters in the path of the incident pump beam, allowing the pump power to be varied from nanowatts to microwatts. Color filters either block or transmit specific wavelengths. These come in a few varieties: high-pass (which allows wavelengths higher than a certain threshold to pass through virtually unaffected), low-pass (which allows wavelengths lower than a threshold wavelength to pass through virtually unaffected), or band-pass (which allows wavelengths within a certain range pass through virtually unaffected). The ND filter was used to reduce the intensity of the laser beam; or to reduce the intensity of the PL signal entering the spectrometer. Color filters were used to block the laser beam's reflection or other stray light from entering the spectrometer, which would thereby either distort the PL spectra or saturate the detector.

Varying the spectrometer's slit widths (entrance and exit) produces several changes in the acquired spectra. The slit width affects the spectrometer's resolution and thus the resolution of the data. As the PL spectra of interest have linewidths much greater than the spectrometer resolution, the slits actually control the amount of light entering the spectrometer and the detector chamber. If the PL was not properly focused into the slits, having the slits closed too tight would prevent any PL from entering the spectrometer even if there is a signal that could be detected. If viewing a weak signal, having the slits too narrow might make the signal-to-noise ratio too small, making the spectra difficult to analyze. Conversely, if measuring a strong signal, having the slits too wide could saturate the detector, or at least push it into the nonlinear regime. Although ND filters could be placed into the system to prevent the latter, sometimes the former would require wide slits. The spectrometer's resolution has been measured using laser lines, which have widths much smaller than 1 nm. As shown in Fig. 4.11(a) and (b), the spectrometer consists of a 0.5 m monochromator

(Acton Spectra Pro 2500i) followed by a liquid-nitrogen-cooled CCD camera. The monochromator has three gratings, with groove densities 600 mm^{-1}, 1200 mm^{-1}, and 1800 mm^{-1}, giving approximate spectral coverage of 50 nm, 20 nm, and 10 nm, respectively. The highest resolution one can obtain with the 1800 mm^{-1}-groove grating is about 0.02 nm. The grating was rotated with high precision by a motor, controlled by a program through a computer. A mechanical shutter between the monochromator exit and the CCD camera was used to control exposure times. The light was sent to the monochromator using focusing lens. Since a typical entrance slit width for the highest resolution was only 15 μm, when collecting emission from objects containing several hundred quantum dots, the emission spectrum had a broadband appearance. In this case, all we can see is the overall distribution of quantum-dot emission energies.

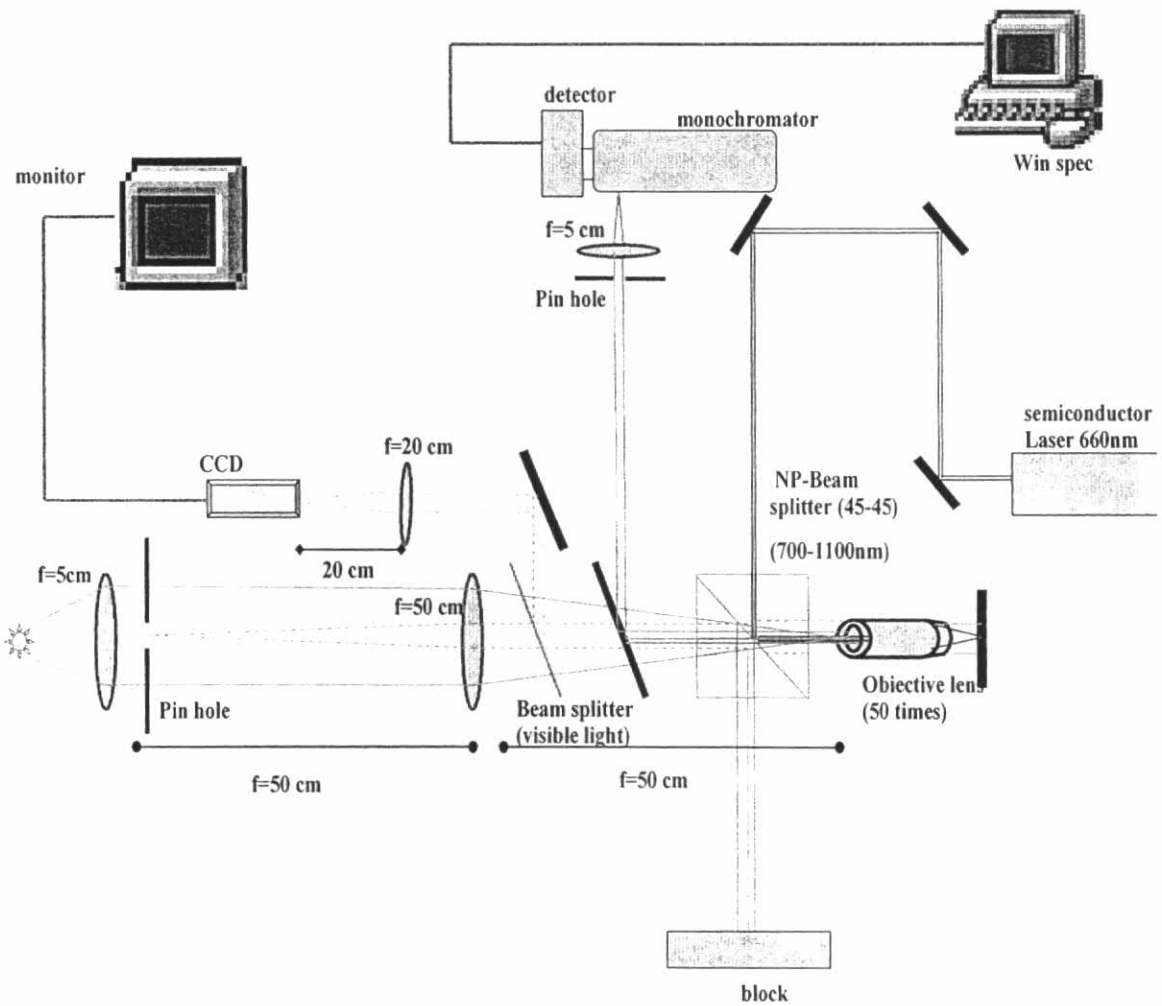

Figure 4.10 A schematic diagram of the micro-PL setup.

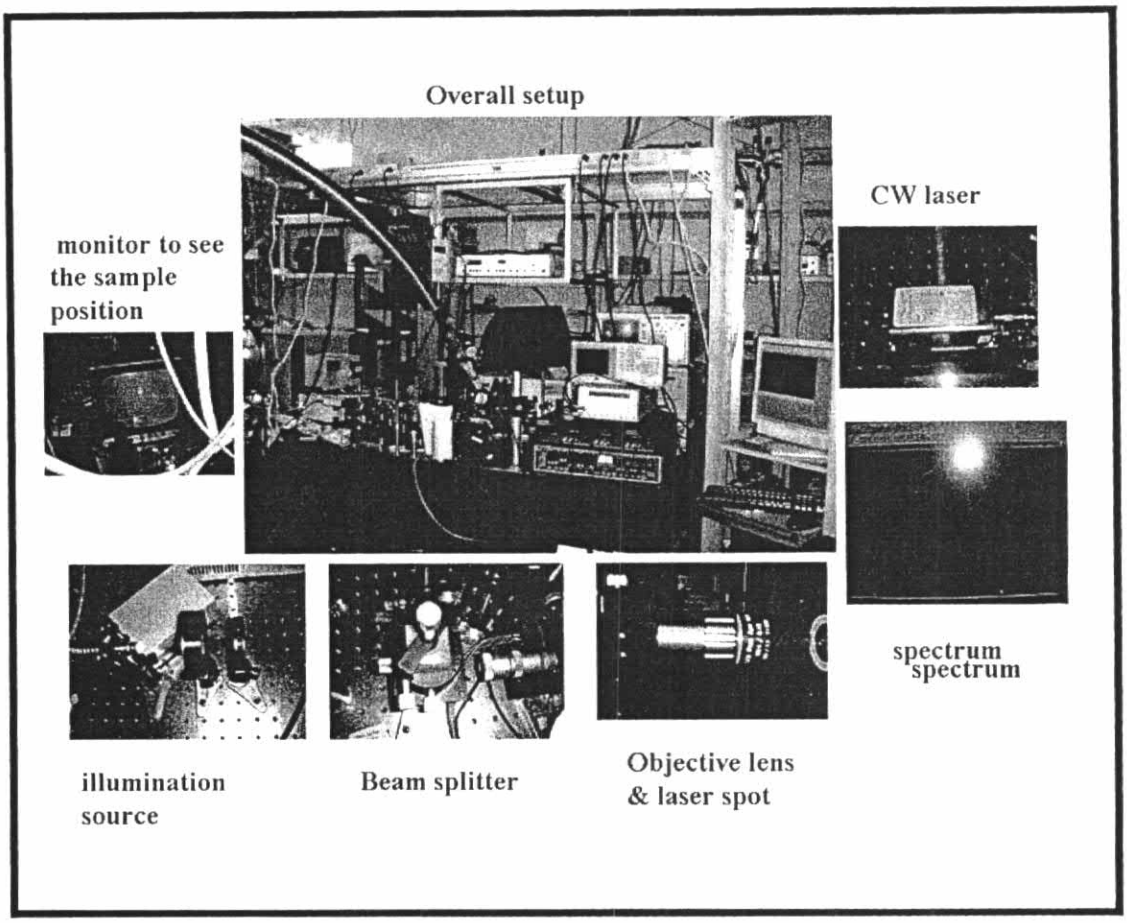

Figure 4.11(a) Photo of the micro-PL setup and its components.

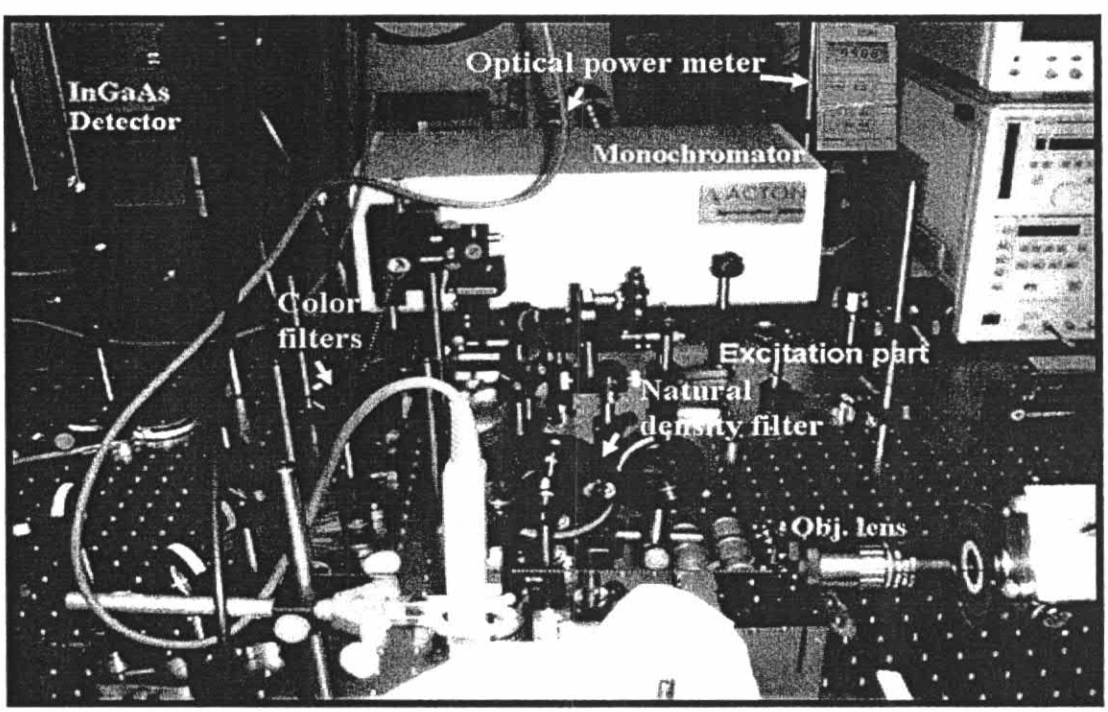

Figure 4.11 (b) Close-up photo of the micro-PL setup and its components.

4.4.3 Temperature Effect

An advantage of room-temperature measurement was that it can allow samples to be changed easily. These features are important for systems used in sample quality control. However, many effects in semiconductor materials can be examined only at cryogenic temperatures. For instance, phonon scattering reduces the lifetime of the carriers so that room-temperature PL of excitons is not possible. The linewidth of the PL is also broadened by these same effects for quantum-dot structures. Hence, it is practical to have the experimental arrangement such that either rapid room-temperature or more sensitive low-temperature measurements can be made. Using the aforementioned lens pair for the PL beam allowed minimal changes in the experimental layout when changing from one temperature measurement to the other, as demonstrated in the following Fig. 4.12.

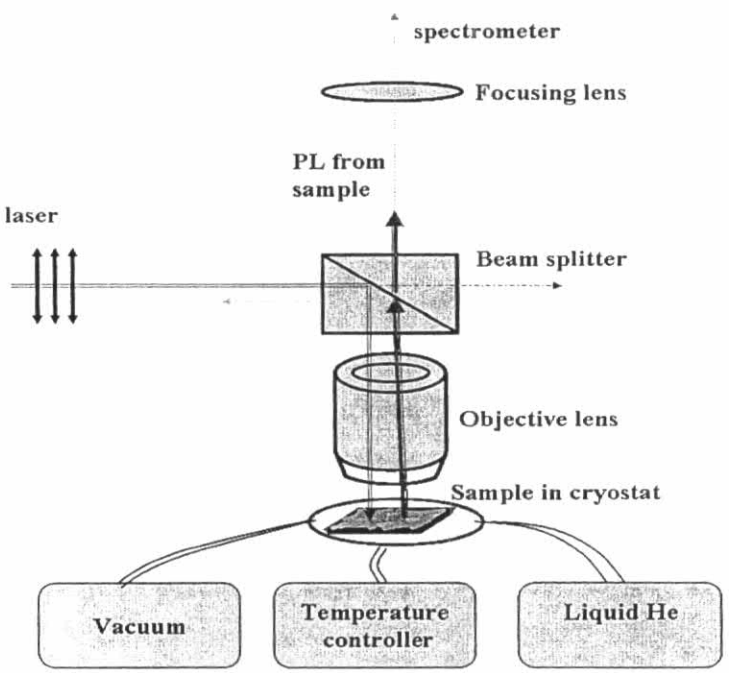

Figure 4.12 Schematic diagram of a setup for the temperature-dependent measurement.

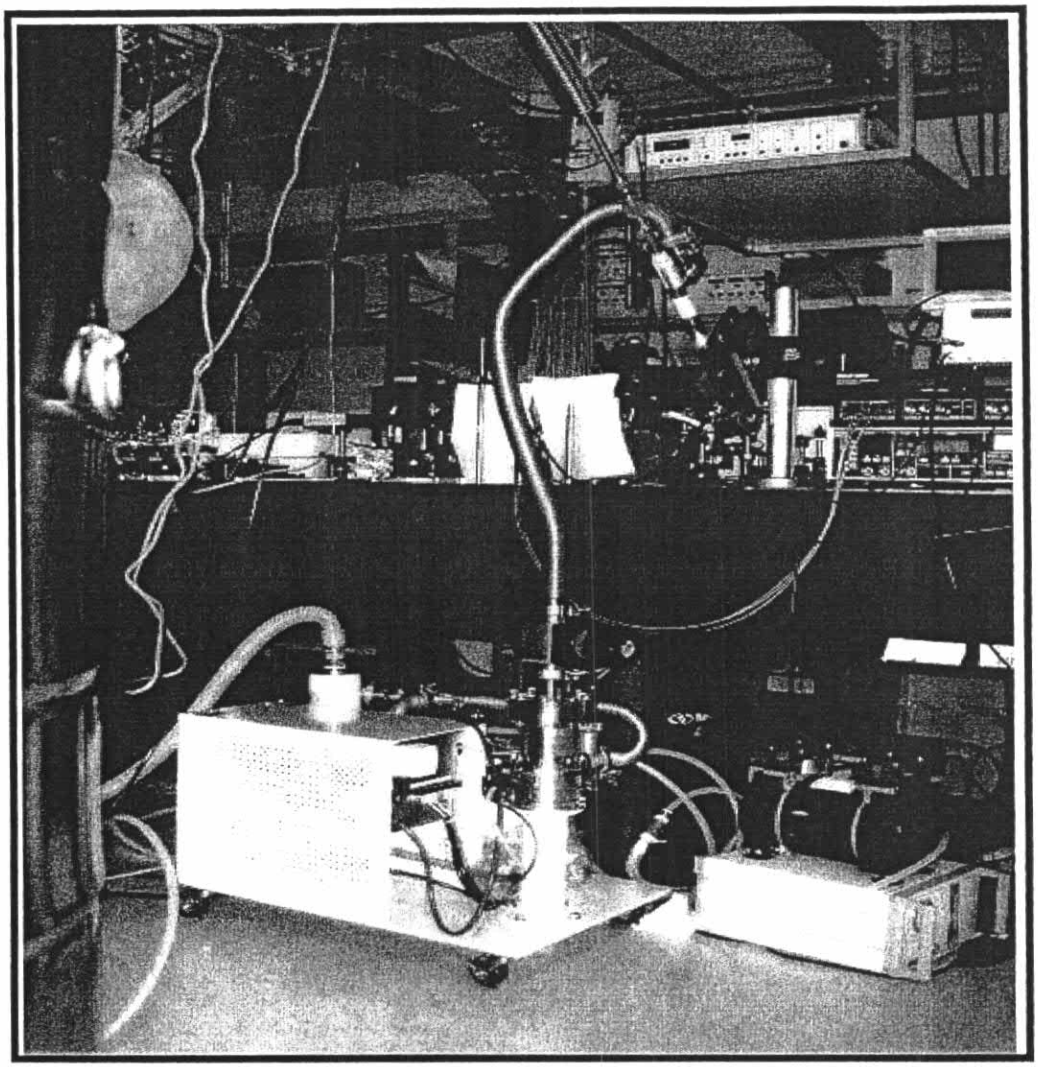

Figure 4.13 Photo of the temperature-dependent PL setup.

The temperature, monitored with a sensor mounted on the cold-finger, was controlled via Oxford 5035 Intelligent Temperature Controller, which was using a programmable integrate/differentiate circuit to supply current to a heater assembly which was also mounted on the cold-finger. This arrangement is depicted in Fig. 4.13. When the temperature was increased from 4 K to a higher temperature, there was some contamination around the optical window of the cryostat caused by the temperature increase. To get rid of this effect, the vacuum system was connected to the cryostat and used to pump out the contamination from the cryostat.

4.5 Polarized-PL Measurements

This measurement was one of the crucial measurements for characterizing the laterally aligned quantum dots. This section discusses some aspects of the components that were added to the previous experimental setup which affect the outcome and repeatability of the experiments. They will be described in relation to different aspects of the experimental layout: the laser light, the optics, the detection, and the sample chamber. Before discussing the experimental layout, some theoretical background for the polarization measurements will be presented.

4.5.1 Malus's law

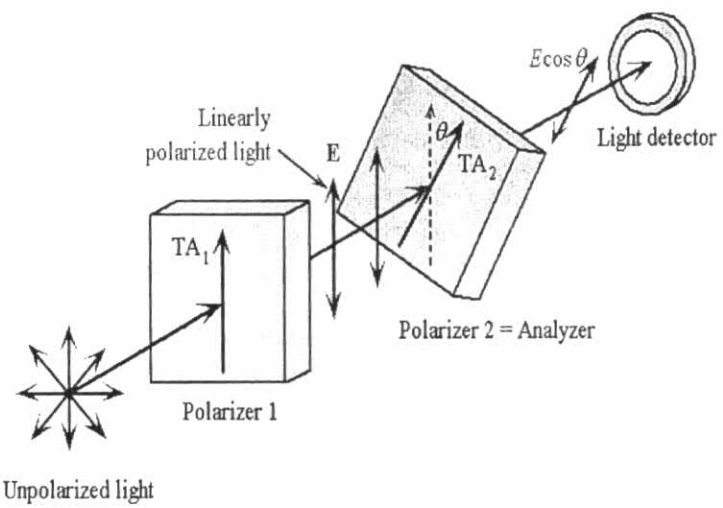

Figure 4.14 Explanation for linear polarization (After Ref. [65])

In Fig 4.14, randomly polarized light is incident on a polarizer 1 with a transmission axis TA1. Linearly polarized light from the polarizer is then incident on the analyzer. By rotating the transmission axis of the second polarizer, the polarization state of the incident beam can be analyzed. If the transmission axis of the second polarizer is at an angle θ to the field of the incident beam, then only the component of the $E \cos \theta$ will be allowed to pass through the polarizer 2. The intensity of light passing through the analyzer is proportional to the square of the electric field [65].

$$I = I_0 \cos^2 \theta \tag{4.4}$$

Therefore, the Malus's law relates the intensity of a linearly polarized light passing through a polarizer to the angle between the transmission axis and the electric field vector. This law was used to analyze the experimental results to confirm degree of linear polarization of the laterally aligned quantum dots investigated in this work.

4.5.2 Polarized-PL Experimental Setup

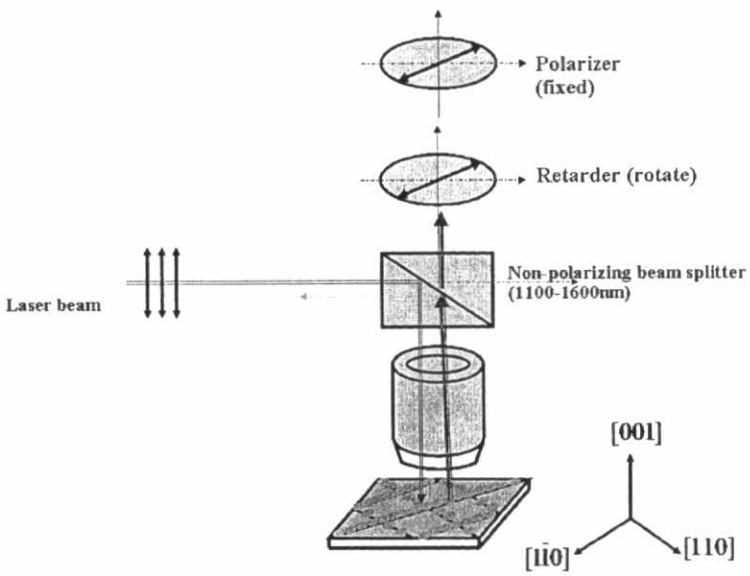

Figure 4.15 Experimental setup for polarization measurements.

The PL spectrum was collected by the objective lens, dispersed by the double-grating monochromater, and detected by an InGaAs detector, the same setup as mentioned before. The polarization characteristic measurement was carried out by fixing a polarizer, serving as the analyzer, which was placed in front of a detector. The output intensity of the detected signal from the photodetector was also displayed by a digital multimeter. To eliminate the artifacts from polarization-dependent efficiency of the monochromator, a half-wave plate was put in front of the monochromator. In the measurement, the transmission axis of the half wave plate was rotated until a maximum reading on the multimeter was obtained, and this was marked as the 0° polarization angle, which was used as the reference angle.

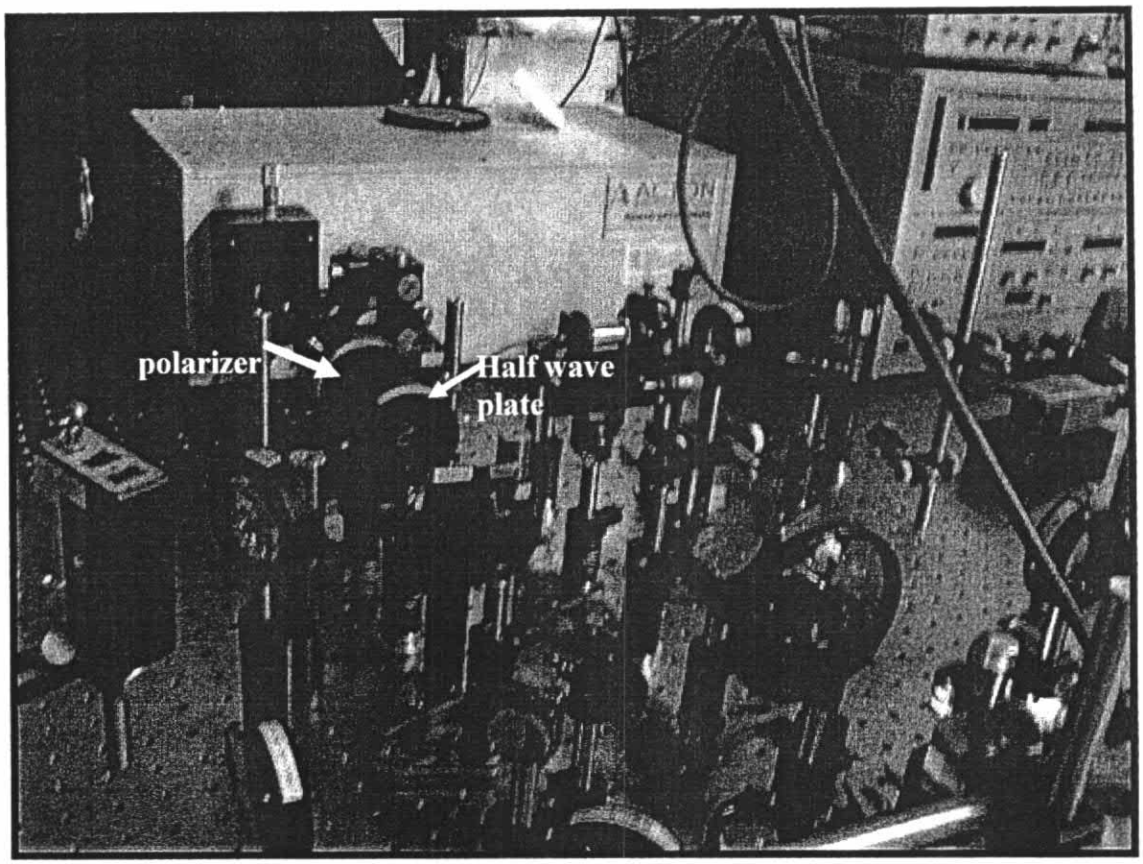

Figure 4.16 Photo of the polarization measurement setup.

In summary, many different factors contribute to the appearance of PL spectra. PL spectra can identify poor crystallinity by emitting weaker intensity. Another interesting behavior in PL spectroscopy is the full-width-at-half-maximum (FWHM) of the PL spectrum. This is because the FWHM may easily become broadened by structural impurities, such as interface roughness, composition, inhomogeneity, and partial strain relaxation, etc. A narrower PL peak can indicate a higher quality sample. However, identified PL behaviors overlap with other causes besides impurities. For instance, broadening, intensity reduction, and energy peak shifting can indicate strain relaxation. On the other hand, growth temperatures and laser excitation power can influence a peak shift to higher energy. The factors are summarized in the following table.

FWHM depends on	Peak energy depends on	Intensity of sample depends on
Temperature	Bandgap energy of material	Excitation laser power
Impurity concentration	Quantum confinement of the structure	Measurement temperature
Dot size homogeneity	Size of the nanostructure	Spectrometer slit width
Exciton binding energy	Measurement temperature	Alignment of the optical setup
Strain relaxation	Strain	
Sample quality		

In conclusion, PL spectroscopy is a useful, nondestructive technique which can be used to determine optical characteristics of the sample under investigation.